Harnessing combinational phototherapy via post-synthetic PpIX conjugation on nanoscale metal-organic frameworks

Journal of
Materials Chemistry B

Materials for biology and medicine

Accepted Manuscript

This article can be cited before page numbers have been issued, to do this please use: R. Chen, W. Chen, Y. Li, S. Tian, B. Liu, X. Chen, C. Lee and W. Zhang, *J. Mater. Chem. B*, 2019, DOI: 10.1039/C9TB01154D.

ROYAL SOCIETY OF CHEMISTRY

rsc.li/materials-b

View Article Online
DOI: 10.1039/C9TB01154D

ARTICLE

Harnessing combinational phototherapy via post-synthetic PpIX conjugation on nanoscale metal-organic frameworks

Received 00th January 20xx,
Accepted 00th January 20xx

DOI: 10.1039/x0xx00000x

Rui Chen, [a] Wen-Cheng Chen, [b] Li Yan, [a] Shuang Tian, [b] Bin Liu, [a] Xianfeng Chen, [c] Chun-Sing Lee [b] and Wenjun Zhang*[a]

Nanomaterial-mediated phototherapy, including photodynamic therapy (PDT) and photothermal therapy (PTT), is an effective anticancer intervention that relies on light activation of photoactive nanomaterials localized in tumors. Recently, combinational PDT/PTT offered a practical pathway to relieve resistance of monotherapy, surmount undesirable side effect and provide synergistic effect to nhance phototherapeutic efficiency. Herein, we report a facile strategy to integrate protoporphyrin IX (PpIX) to nanoscale metal-organic frameworks (NMOFs) and control their photoactive properties for combinational cancer PDT and PTT. With optimized PpIX conjugation, the as-fabricated nanoparticles (nPCU NPs) exhibit (1) improved dispersibility and particle stability; (2) simultaneous generation of reactive oxygen species and heat effectively through activation by single-wavelength laser of 635 nm; (3) maintenance of porosity for further application as drug delivery vehicles. Moreover, *in vitro* investigation of nPCU NPs demonstrates effective cellular uptake, successful endosomal escape and enhanced phototherapeutic efficacy under both normoxic and hypoxic conditions. Therefore, this study developed a novel type of phototherapeutic nanoplatforms with optimal properties for applicable cancer phototherapy.

Introduction

Phototherapy, including photodynamic therapy (PDT) and photothermal therapy (PTT), has been considered as non-invasive and applicable therapeutic intervention against cancers.[1,2] For typical PDT, photosensitizers (PSs) are activated by illumination of light and transfer their energy to molecular oxygen and substrates, which generates cytotoxic reactive oxygen species (ROS) to kill cancer cells.[3,4] While PTT employs photothermal agents to convert absorbed light into heat, consequently leading to localized hyperthermia and thermal ablation of tumors.[5,6] Over the past few decades, a variety of photoactive nanoparticles (NPs) have been extensively explored as PDT or PTT agents owing to their passive and possibly active targeting ability upon abnormal tumor vasculature.[7–12] However, it has been recognized that tumor heterogeneity and microenvironment severely compromise preclinical and clinical treatment outcomes of either PDT or PTT.[13,14] Furthermore, both PDT and PTT are subject to safety concern of high-power laser irradiation and massive dose of photoactive nanomaterials.

To overcome the aforementioned limitations and improve therapeutic efficacy, an appealing approach in recent research is to integrate PDT or PTT with other therapeutic modalities such as chemotherapy, which generates multiple mechanisms for enhanced cancer therapy.[15–19] Nevertheless, incorporation of anti-cancer drugs to phototherapeutics not only increase structural complexity, but also arouse concerns with regard to drug delivery issues such as low drug loading capacity, premature release, and associated toxicity.[20] As another optional strategy, combination of PDT and PTT into a nanoplatform provides a promising pathway to exert synergistic photothermal and photodynamic effect with less dose of nanomaterials and irradiation. Upon preferable single-laser irradiation, the simultaneous production of ROS and hyperthermia can effectively mediate tumor microenvironment to activate anti-tumor response upon other therapeutics.[21,22] Although some organic and inorganic nanomaterials witnessed success in combinational PDT and PTT,[23–28] these formulations still face challenges to simplify synthetic process, employ single-wavelength laser, and finely control fractions of PDT and PTT to maximize treatment outcomes.

Nanoscale metal-organic frameworks (NMOFs), which are constructed by assembling metal ions or metal clusters and organic linkers, represent a potent type of porous nanocarriers and have received considerable explorations in drug delivery.[29–31] Recently, broad interest has been spent on porphyrin NMOFs comprising large quantity of photoactive porphyrin for PDT.[32–37] On the other hand, incorporating other photoactive nanomaterials such as gold nanorods, polyaniline and porphyrin polymers to NMOF nanostructures has been employed to develop novel nanohybrids for phototherapy.[38–40] However, by now, few study focused on controlling photoactive properties of NMOFs for combinational PDT and PTT.

In this study, we describe a facile strategy to post-synthetically modify NMOF templates with protoporphyrin IX (PpIX). The as-synthesized PpyIX conjugated NMOFs (nPCUs) represent a tunable

[a] Center of Super-Diamond and Advanced Films (COSDAF), Department of Materials Science and Engineering, City University of Hong Kong, Hong Kong SAR, P. R. China.
E-mail: apwjzh@cityu.edu.hk
[b] Center of Super-Diamond and Advanced Films (COSDAF), Department of Chemistry, City University of Hong Kong, Hong Kong SAR, P. R. China.
[c] School of Engineering, Institute for Bioengineering, The University of Edinburgh, King's Buildings, Mayfield Road, Edinburgh EH9 3JL, UK.
Electronic Supplementary Information (ESI) available: See DOI: 10.1039/x0xx00000x

View Article Online
DOI: 10.1039/C9TB01154D

combination of PDT and PTT by varying conjugation amounts of PpIX, which is attribute to a π-stacking effect of PpIX within the struts of NMOFs. Consequently, we optimize combinational PDT and PTT effect of nPCUs and demonstrate the NPs as a novel phototherapeutics with good potential for preclinical and clinical applications.

Experimental

Materials

Zirconium chloride anhydrous ($ZrCl_4$), protoporphyrin IX (PpIX), acetic acid, cobalt dichloride, dichloromethane (CH_2Cl_2), oxalyl chloride, 2',7'-dichlorofluorescein diacetate (DCFH-DA), dimethylformamide (DMF), tetrahydrofuran (THF), ethanol, methanol were purchased from Sigma-Aldrich. 2'-amino-terphenyl-4,4''-dicarboxylic acid (TPDC-NH_2) was synthesized according to the reported reference.[41] Fetal bovine serum (FBS), phosphate buffered saline (PBS), Dulbecco's modified Eagle medium (DMEM), penicillin streptomycin 10,000 U/mL (PS), trypsin, calcein acetoxymethyl ester (calcein-AM), propidium iodide (PI), and Hoechst 33422 were ordered from Invitrogen. Low viscosity embedding media spur's kit was purchased from Electron Microscopy Sciences. Unless otherwise noted, all chemicals were used without further purification.

Characterizations

Scanning electron microscope (SEM) images were acquired with a Philips XL-30 FEG scanning electron microscope. Transmission electron microscope (TEM) images were obtained with a FEI/Philips Tecnai 12 BioTWIN transmission electron microscope. Powder X-ray diffraction (PXRD) was recorded with a Siemens D500 X-Ray Diffractometer with Cu Kα radiation source (λ =1.5406 Å). Dynamic light scattering and zeta potential measurements were conducted on a Malvern Zetasizer Nano ZS instrument. Ultraviolet-visible absorption spectra were recorded with SHIMADZU 1700 Ultra-Violet Visible Scanning Spectrophotometer. Photoluminescence spectra were measured with a HORIBA FluoroMax-4 steady state spectrophotometer. Optical and fluorescent observation of cells were carried on a Nikon ECLIPSE FN1 microscope equipped with an ANDOR Zylar sCMOS camera. Confocal laser scanning microscope (CLSM) images were obtained from Leica TCS SP5 laser confocal scanning microscope. The irradiation source of singlet oxygen quantum yield, photothermal conversion efficiency measurements and in vitro experiments was a 635-nm laser equipped with uniformity modulator, which has maximal output power of 2W.

Synthesis of nUiO-68-NH_2 NPs

A facile solvothermal reaction between metal precursor solution and organic linker solution was employed to synthesize nUiO-68-NH_2 NPs ("n" denotes nanoscale, and "UiO" denotes Universitetet i Oslo). Briefly, the metal precursor solution was prepared by dissolving 15 mg $ZrCl_4$ in 10 mL DMF. To prepare the organic linker solution, 19 mg TPDC-NH_2 and 1.35 mL acetic acid were dissolved in 10 mL DMF and 0.2 mL H_2O (increasing amount of H_2O will improve the yield of NPs but exacerbate their crystallinity). Next, the two solutions were mixed by ultrasonication, and the mixture of 20 mL solution was transferred into a Teflon-sealed autoclave and kept at 90 °C for 48 hours. The formed nanoparticles were collected by centrifugation at 7000 rpm for 20 minutes, then washed repeatedly with DMF, methanol and THF.

Preparation of nPCU NPs

PpIX molecules were chlorinated before being conjugated to nUiO-68-NH_2 NPs(Scheme S1).[42] 0.1 mmol (56.3 mg) PpIX and 100 μL oxalyl chloride were mixed together in 50 mL CH_2Cl_2, and 20 μL DMF was added dropwise to form a clear solution. The mixed solution was stirred for 2 hours at room temperature, followed by evaporation with N_2 flow and being stored in 100 mL THF at a concentration of 1 μmol/mL. Next, 0.2, 0.4, 1, 2, 4, 5 μmol PpIX chloride and 5 mg nUiO-68-NH_2 in 20 mL THF were stirred with reflux at 60 °C for 12 hours. The resulted nPCUx NPs (x denotes weight percent of PpIX in the NPs) were isolated by centrifugation and washed with THF, methanol several times. To quantify conjugated PpIX, UV-vis absorption spectra was utilized to determine the concentrations of PpIX chloride. Accordingly, the conjugation efficiency and content of PpIX was calculated as follows:

$$\text{Conjugation efficiency} = \frac{m(\text{reactant}) - m(\text{supernatant})}{m(\text{reactant})} * 100\%$$

$$\text{Conjugation content} = \frac{m(\text{reactant}) - m(\text{supernatant})}{m(\text{nPCUx})} * 100\%$$

Where *m*(reactant) denotes weight amount of PpIX chloride added in reaction, *m*(supernatant) stands for weight amount of PpIX chloride in supernatant after reaction.

Singlet oxygen generation of laser-irradiated nPCU NPs

Singlet Oxygen Sensor Green (SOSG) were respectively mixed with 50 μg nUiO-68-NH_2 and nPCU NPs at final concentration of 5 μM. A control group was set without any NPs added. The three solutions were irradiated with a 635-nm laser at 1W/cm^2 for 4 min. Fluorescence intensity of SOSG excited at 490 nm were recorded at a time interval of 1 min. All the recorded intensities of three groups subtracted their initial intensity, followed by being plotted with irradiation time.

Temperature profiles of laser-irradiated nPCU NPs

Firstly, 1 mL 50, 100, 200 μg/mL nPCU NPs in water were exposed to a 635-nm laser at a power density of 1 W/cm^2 and spot size is 1.15 cm^2. Then, 1 mL 100 μg/mL nPCU NPs was exposed to laser irradiation of different power density at 0.3, 0.6, 1.2 and 1.8 W/cm^2. The temperature measurements were acquired every 30 seconds using an RS Pro Digital Thermometer.

Photothermal conversion efficiency of nPCUx NPs

The photothermal conversion efficiencies of nPCUx NPs were determined according to the reported method.[43] In brief, 100 μg nPCUx NPs were dispersed in 1 mL aqueous solutions and their absorbance at 635 nm were measured by UV-vis spectrophotometer. All the above samples were irradiated with a 635-nm laser at power density of 1 W/cm^2. Then the laser was shut down to cool down the

View Article Online DOI: 10.1039/C9TB01154D

solutions to ambient temperature. The temperatures at cooling stage were recorded at a time interval of 30 seconds. Time (t) versus negative Napierian logarithm of the temperature driving force ($\ln(\vartheta)$) of different samples were plotted. Following the calculation method, we obtained the photothermal conversion efficiencies (η) of nPCUx NPs.

Singlet oxygen generation efficiency of nPCUx NPs

For measuring singlet oxygen generation efficiency of nPCUx NPs, we followed the method by using singlet oxygen sensor green (SOSG) and methylene blue (MB) as indicator and reference.[32] In brief, 100 μL 15 μM SOSG methanol solution was mixed to 3 mL nPCU NPs and MB water solution. The absorption peak at 635 nm of nPCU NPs were adjusted to be optical density of 0.2. After being irradiated at time interval of 1 minutes, the fluorescence intensity of SOSG at 525 nm (excited at 490 nm) was recorded with increasing irradiation time. The data was respectively fitted with the equation:

$$I = A(1 - e^{kt})$$

Where I is fluorescence intensity of SOSG and t is irradiation time, A and k are fitting parameters obtained from nonlinear curve fit (BoxLucas1) by Origin. The product of Ak in the equation indicates the singlet oxygen generation efficiency. The fitting parameters and singlet oxygen generation efficiency were listed in Table S2.

Doxorubicin loading by nPCU NPs

As the absorption of DOX is linearly proportional to its concentration, a standard curve was carried out by UV-vis absorption spectrometer. DOX-loaded nPCU NPs were prepared by simply immersing 1 mg NPs in 1 mL water solution with 1 mg/mL DOX. After 1 day, nPCU/DOX NPs were collected by centrifugation. And the unloaded DOX in supernatant was quantified by the obtained standard curve. The loading efficiency and capacity of DOX in nPCU/DOX NPs was calculated according to the following equation:

$$\text{Loading efficiency} = \frac{m(\text{DOX})\ \text{initiation} - m(\text{DOX})\ \text{supernatant}}{m(\text{DOX})} * 100\%$$

$$\text{Loading capacity} = \frac{m(\text{DOX})\ \text{initiation} - m(\text{DOX})\ \text{supernatant}}{m(\text{nPCU/DOX NPs})} * 100\%$$

Cell culture

Human epithelial lung carcinoma (A549) and glioblastoma brain carcinoma (LN229) were cultured in DMEM medium supplemented with 10% FBS and 1% PS in a humid atmosphere with 37 °C and 5% CO_2. A549 cells under normoxic and hypoxic conditions were obtained by inducing them with complete medium containing 250 μM $CoCl_2$ for 4 hours.

***In vitro* cell imaging of nPCU/DOX NPs**

To prepare imaging samples, A549 cells were cultured in glass-bottomed dishes with 2 mL medium, then mixed with nPCU/DOX NPs dispersed in DMEM to maintain a concentration of 20 μg/mL. After being incubated for 12 hours, the cells were stained by Hoechst 33342 (10 μM) for 10 min and fixed at 37 °C under 5% CO_2 atmosphere. A control sample was prepared identically without adding any NPs. Under fluorescence microscope, Hoechst 33342 was excited at 700 nm (two-photon) and the blue emission was collected inthe range of 435-480 nm. NPs was excited at 543 nm and red emission was collected in the range of 605-660 nm.

***In vitro* phototherapy of nPCU NPs**

The cytotoxicity of nPCU NPs was evaluated by standard 3-(4,5-dimethylthialzol-2-yl)-2,5-diphenyltetrazolium bromide (MTT) assay on A549 and LN229 cells. Cancer cells were seeded and incubated for one day. Then, nPCU NPs were added into different groups of cells. For phototherapy, when incubated for 12 hours, irradiation groups were exposed to 635-nm laser at 100 mW/cm^2 for 3 minutes. After another incubation time of 12 hours, the cells were incubated with fresh DMEM supplemented with PS and 0.5 mg/mL of MTT, followed by 4-hour incubation. Finally, the medium in each well was replaced by 200μL DMSO. A micro-plate reader was used to measure the absorbance at 490 nm. To avoid random error, every group with a certain NP concentration was averaged from five parallel experiments.

To support the results of phototherapy by visualized images, A549 cells were treated with irradiation of 635-nm laser at 100 mW/cm^2 for 3 minutes, 5 μg/mL nPCU NPs, and 5 μg/mL nPCU NPs with the irradiation respectively. Then the cells were co-stained with calcein-AM (5 μmol, emission: 515 nm) and PI (5 μmol, emission: 617 nm) and observed via CLSM with excitation of 488 nm.

***In vitro* phototherapy of PpIX and nPCU NPs under normoxic and hypoxic conditions**

As PpIX molecules were nearly insoluble in aqueous solution, we firstly prepared 4 mg/mL PpIX DMSO solution and diluted it with cell medium into final concentration for experiments (DMSO solvent was added to keep it equivalent in all experimental groups). It was also found that PpIX had strong cytotoxicity after incubating with cells overnight. To compare the therapeutic efficiencies of NPs and PpIX, the incubation time was reduced. Specifically, all groups of A549 cells were seeded and incubated with normal cell medium for one day. Then the cells were incubated with PpIX and nPCU NPs in normal cell medium (normoxia) and cell medium with 250 μM $CoCl_2$ (hypoxia) for 4 hours. The cell medium was replaced with fresh one before being irradiated with 635-nm laser at 50 mW/cm^2 for 3 minutes. After further incubation for 2 hours, MTT assay was employed to evaluate phototherapeutic efficiencies of all studied groups.

Intracellular ROS generation

The intracellular ROS generation was detected by CLSM using DCFH-DA as indicator. A549 cells with proper density were incubated with 3 μg/mL PpIX and nPCU NPs in cell culture medium. For hypoxia, the cell medium contained 250 μM $CoCl_2$. After incubation for 4 hours, the cell medium was replaced with a fresh one and the cells were irradiated with 635 nm laser at 50 mW/cm^2 for 3min. Then, the cells were incubated with DCFH-DA (25 μM, PBS) in the dark for another 20 min. The DCFH-DA solutions were removed and the cells were washed with PBS for two times before observation with CLSM. The images were acquired with an excitation of 488 nm and emission range of 515-525 nm.

Results and discussion

Preparation and characterization of nPCU NPs

The amine-tagged NMOFs, nUiO-68-NH_2 ("n" denotes nanoscale, "UiO" denotes Universitetet i Oslo and "-NH_2" symbolizes primary amine), were firstly synthesized as templates to conjugate PpIX molecules because of their strong coordination bonds, abundant available amino groups and large octahedral voids of 25.6 Å.[41] These properties are much beneficial to maintaining structural integrity and stability during post-synthetic modification. As depicted in **Fig. 1a**, amine-tagged NMOFs nUiO-68-NH_2 were synthesized through solvothermal reaction of zirconium (IV) chloride and TPDC-NH_2 in DMF at 90 °C, modulated by acetic acid. To attain stable and specific binding, PpIX were chlorinated, then reacted with nUiO-68-NH_2 to construct PpIX-conjugated nUiO-68 (nPCU) NPs (**Scheme S1**). By tuning PpIX amount in the conjugation reaction, nPCU NPs with various PpIX contents are obtained (**Table S1**). Considering the maximal conjugation content of 29.1wt% and large pore size of nUiO-68, the PpIX molecules are believed to bind to the amines both within and onto framework structure of the NPs. Subsequently, all studies were performed on the nPCU NPs containing 29.1 wt% PpIX if weight percentage is not indicated.

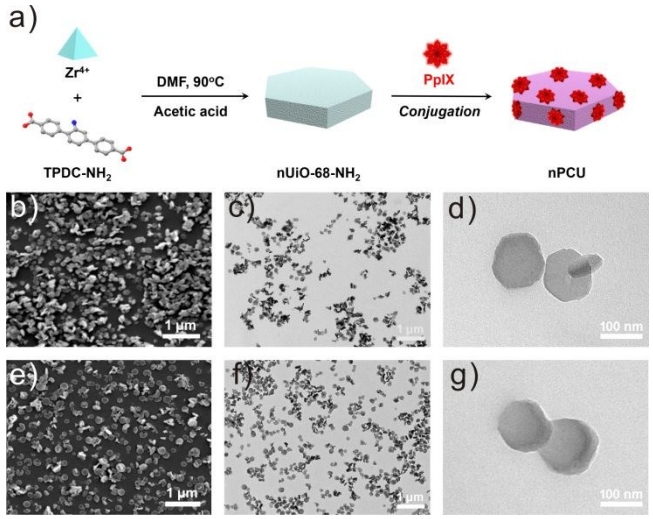

Fig. 1 a) Schematic illustration showing synthesis of nPCU NPs. TEM images of b) nUiO-68-NH_2 and c) nPCU NPs. d) PXRD patterns of nUiO-68-NH_2 and nPCU NPs. e) Zeta potentials of nUiO-68-NH_2 and nPCU NPs. DLS size profiles of nUiO-68-NH_2 and nPCU NPs by f) intensity and g) number.

Transmission electron microscopy (TEM) images in **Fig. 1b** reveal that nUiO-68-NH_2 NPs have a typical morphology of hexagonal nanoplates with a size of ~120 nm in diameter and ~20 nm in thickness. With maximum of PpIX conjugated, nPCU NPs remain a similar morphology as disclosed in **Fig. 1c**.

Powder X-ray diffraction (PXRD) patterns of the as-prepared nPCU in **Fig. 2a** are almost identical to those of nUiO-68-NH_2 NPs and previously reported UiO-68-NH_2.[44] Furthermore, the zeta potentials of nUiO-68-NH_2 changes from 15.8 mV to -22.6 mV after PpIX conjugation (**Fig. 2b**), which indicates positively charged amines on the surface of NPs are successfully grafted with PpIX molecules in nPCU NPs. Meanwhile, from dynamic light scattering (DLS) profiles in **Fig. 2c** and **2d**, the hydrodynamic intensity sizes of nUiO-68-NH_2 and nPCU NPs are 314.9 and 252.9 nm, whereas their number sizes are 156.8 and 195.2 nm, respectively. With reference to nPCU NPs, the reduced intensity size of nPCUs is ascribed to a better dispersity, evidenced by their smaller polydispersity index (PDI). While the increase of number size verifies successful PpIX conjugation on the surface of NPs. Therefore, the proposed PpIX conjugation method is feasible and nondestructive to structural integrity and crystallinity of NMOF templates.

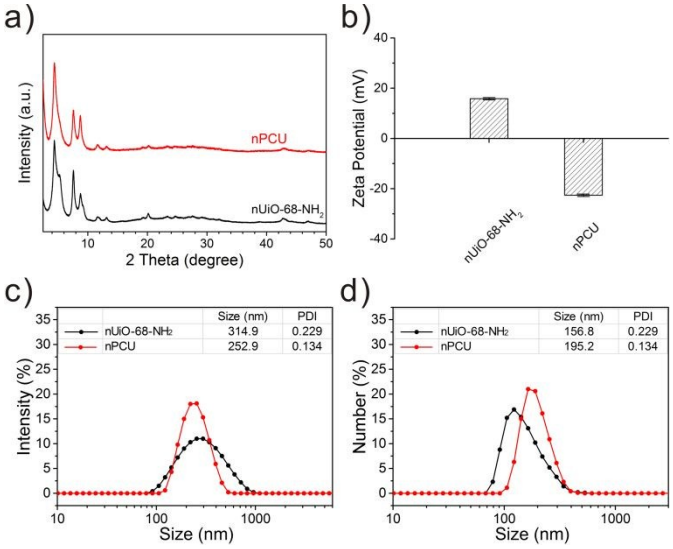

Fig. 2 a) PXRD patterns of nUiO-68-NH_2 and nPCU NPs. b) Zeta potential of nUiO-68-NH_2 and nPCU NPs in water (each group contains three samples). DLS size distributions of nUiO-68-NH_2 and nPCU NPs by c) intensity and d) number.

Good size stability of nanomaterials in aqueous solution is one of prerequisites for significant cellular uptake and tumor accumulation. **Fig. S1** shows that nUiO-68-NH_2 NPs are unstable and quickly agglomerate which is induced by electrostatic interactions between amines and uncoordinated carboxyl groups on the surface of NPs. In contrast, nPCU NPs have minimal Z-average size change during one-week dispersion in water and cell culture medium. The conjugated PpIX molecules substitute amines of NMOFs to prevent the interaction among NPs and improve their aqueous stability for biomedical use.

Tunable photoactive properties of nPCU NPs

Next, the absorption and photoluminescence of nUiO-68-NH_2 and nPCU NPs were studied. As shown in **Fig. 3a**, the absorption spectrum of nPCU NPs integrate those of PpIX and nUiO-68-NH_2 NPs, but distinctively display a bathochromic shift together with broadening bands. In addition, the photoluminescence of nPCU NPs at 630 and 645 nm become weaker with increasing PpIX conjugation content (**Fig. S2**). These spectra variations suggest formation of PpIX aggregates with strong π-stacking effect, which could potentially transform the energy dissipation of absorbed light from photoluminescence to non-irradiative pathway such as heat.[45,46]

View Article Online
DOI: 10.1039/C9TB01154D

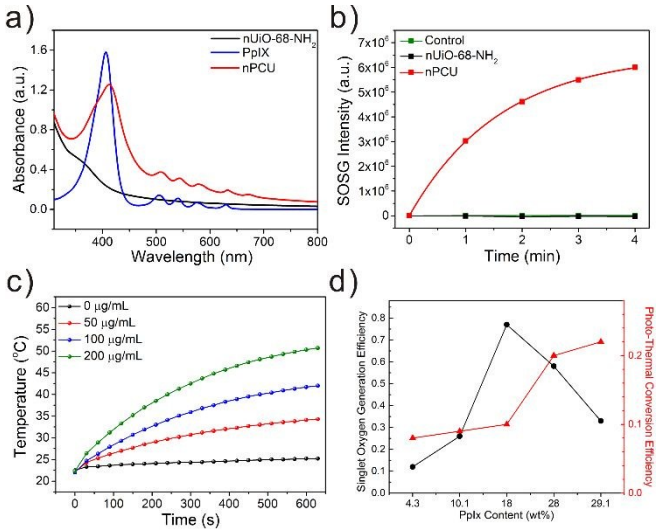

Fig. 3 a) Absorption spectra of nUiO-68-NH_2, PpIX and nPCU NPs in DMF. b) Singlet oxygen generation of nUiO-68-NH_2, nPCU NPs and control group irradiated with a 635-nm laser at 1 W/cm^2. c) Temperature elevation of nPCU NPs at various concentrations under the irradiation. d) Singlet oxygen generation efficiency (black circle) and photo-thermal conversion efficiency (red triangle) of nPCU NPs with various PpIX conjugation contents.

To investigate the photoactive properties of nPCU NPs, we firstly measured their singlet oxygen generation capacity. For comparison, nPCU, nUiO-68-NH_2 and control group were individually mixed with equivalent SOSG and then exposed to a 635-nm laser. Only nPCU NPs show an obvious green fluorescence increase (**Fig. 3b**), indicating they can generate singlet oxygen from ambient molecular oxygen when activated by laser irradiation. Besides, photothermal property of nPCU NPs was evaluated by monitoring the temperature of the solution with continuous exposure to a 635-nm laser. In **Fig. 3c**, after irradiation for 600 s, the temperature of 200 μg/mL of nPCU NPs increases by 28.0 °C while that of the control group i.e. 0 μg/mL of NPs only increases by 2.7 °C. Therefore, the as-prepared nPCU NPs are able to simultaneously serve as photodynamic and photothermal agents under single-laser irradiation.

The photothermal effect of nPCU NPs originate from π-stacking effect of PpIX, which is dependent on the conjugation content of PpIX to NMOFs. To confirm the tunable photoactive properties of nPCU NPs, we determined singlet oxygen generation efficiency and photo-thermal conversion efficiency of a series of nPCU NPs with different PpIX content of 4.3, 10.1, 18.0, 28.0 and 29.1 wt% according to a previously reported method.[47,48] As shown in **Fig. 3d**, when the PpIX content reached 18 wt%, nPCU NPs show a dominant PDT effect with the highest singlet oxygen generation efficiency of 0.77. Intriguingly, further increasing PpIX conjugation content reduces singlet oxygen generation of nPCU NPs while promoting light-to-heat conversion, which is attributed by enhanced π-stacking effect of PpIX within the NPs. The highest photo-thermal conversion efficiency of 0.22 was observed in nPCU NPs with maximal PpIX content of 29.1 wt%, which is comparable with commercial gold nanoshells (0.13) and gold nanorods (0.21).[49]

Cellular uptake and cell imaging of nPCU NPs

As the fluorescence of nPCU NPs is mostly quenched, we firstly employed TEM to confirm cellular uptake and study ultrastructural localization of the NPs inside human alveolar A549 cells (**Fig. 4a**). After an incubation period of 12 hours, plate-shaped nPCU NPs were found in late exosome fusing with lysosome (blue arrow), lysosome (yellow arrow), and cytoplasm (red arrow), which indicates that these NPs could stably exist inside cells during different stages of endocytosis. We hypothesize that nPCU NPs can escape from endosome/lysosome through two pathways mediated by the proton sponge effect and possible photochemical internalization.[50,51] Specifically, nPCU NPs contain grafted and spare amines of NMOFs, secondary and tertiary amines of conjugated PpIX. These amines can absorb protons inside late endosomes and lysosomes, leading to osmotic pressure increase and membrane disruption. Titration experiment of nUiO-68-NH_2 and nPCU NPs verifies their pH-buffering effect on account of protonation and deprotonation (**Fig. S3**). On the other hand, a little dose of light activation upon nPCU NPs is able to generate localized singlet oxygen to destabilize endosomal membrane and result in release of endocytosed NPs. The prolonged retention of nPCU NPs in cytosol of cancer cells can benefit the efficiency of phototherapy.

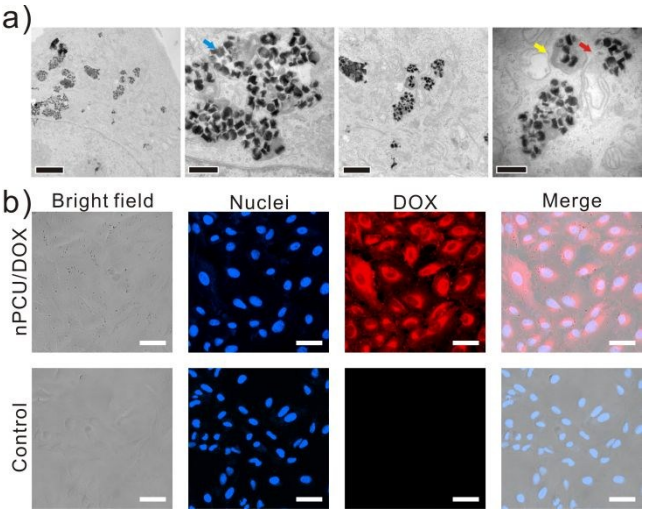

Fig. 4 a) TEM micrographs of A549 cell incubated with nPCU NPs for 12 h, scale bars: 1 μm, 400 nm, 1 μm and 400 nm from left to right. b) CLSM images of A549 cells incubated with and without nPCU/DOX NPs for 12 h. The cell nuclei were stained with Hoechst 33342. Scale bars: 50 μm.

Except large octahedral voids, there are also small tetrahedral voids in the crystalline structure of UiO-68 NMOFs. Those voids are not sufficient to host PpIX, but likely to entrap some anti-cancer drugs with small size. With this consideration, we next examined whether nPCU NPs could encapsulate fluorescent doxorubicin (DOX) for imaging and chemotherapy purpose. Successful DOX loading was confirmed by SEM observation, the characteristic peaks of DOX absorption, and the fluorescence spectra of DOX-loaded nPCU (nPCU/DOX) NPs (**Fig. S4**). The loading efficiency and content of DOX was calculated to be 31.5% and 23.9 wt% respectively. Next, the cellular uptake of nPCU/DOX NPs was observed by confocal laser scanning microscopy. **Fig. 4c** shows the cells contain nPCU/DOX NPs with strong red fluorescence surrounding Hoechst-stained nuclei (blue), implying that the DOX-loaded NPs are internalized to

cytoplasmic region of A549 cancer cells. In contrast, free DOX molecules are prone to enter into and preferentially stain cell nuclei. Hence the photoactive nPCU NPs are validated to possess the capability of entrapping anti-cancer drugs for chemotherapy, which can be leveraged to construct multi-modality therapeutics.

Cytotoxicity and phototherapy of nPCU NPs

Encouraged by prominent internalization behavior of nPCU NPs in vitro, we subsequently test their cytotoxicity and phototherapeutic effect against A549 and LN229 cancer cells using the standard 3-(4,5-dimethylthiazol-2-yl)-2,5-diphenyltetrazolium bromide (MTT) assay. As shown in **Fig. 5a**, high cell viability in laser only control group (Ctrl) suggests that 3-min irradiation with 635-nm laser at 100 mW/cm^2 does not lead to any A549 cell death. Without laser irradiation, A549 cells incubated with nPCU NPs at a maximum concentration of 50 μg/mL have a cell viability of higher than 80%, indicating excellent biocompatibility of nPCU NPs. However, in presence of laser irradiation, discernible cytotoxicity starts to be observed when the concentration of nPCU NPs is over 3.12 μg/mL, and the cell viability dramatically drops to below 20% when the concentration further increases to 6.25 μg/mL. Similar results were also obtained on brain glioblastoma LN229 cancer cells (**Fig. 5b**).

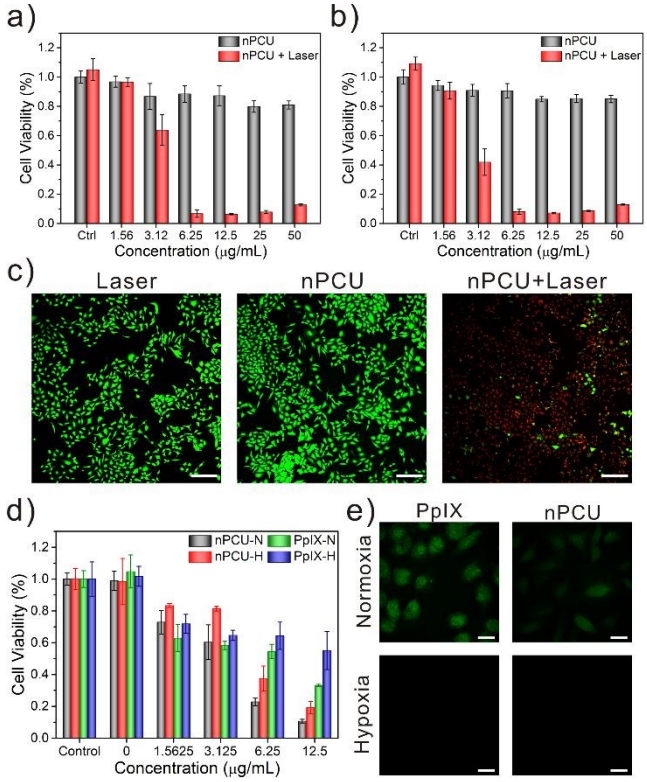

Fig. 5 Cell viabilities of a) A549 and b) LN229 cells after incubated with nPCU NPs at various concentrations in absence and presence of laser irradiation. c) Merged fluorescent images of calcein-AM and PI co-staining A549 cells treated with laser irradiation; scale bars: 200 μm. d) In vitro phototherapy of nPCU NPs and PpIX under normoxic and hypoxic conditions. e) CLSM images of A549 cells treated with PpIX + irradiation and nPCU NPs + irradiation under normic and hypoxic conditions. All the cells were stained with DCFH-DA to detect ROS generation; scale bars: 25 μm. The error bars are obtained by measuring five independent samples in each group of MTT assay.

In addition, live-dead staining with calcein acetoxymethyl ester (calcein-AM) and propodium iodide (PI) was utilized to visualize the therapeutic results via CLSM in **Fig. 5c**. The A549 cells individually treated with irradiation and 5 μg/mL of nPCU NPs predominantly present green fluorescence, indicating negligible cytotoxicity under the used experimental condition. In contrast, combination of laser irradiation and 5 μg/mL of nPCU NPs leads to substantial cell death, revealed by the red fluorescence of PI within the cells.

Hypoxia, as a common feature of many tumors especially in deep tissues, has compelling influences on tumor biology and responses to therapy.[52] For instance, consumption of oxygen and limited oxygen diffusion in hypoxic tumors can severely suppress therapeutic effect of PDT.[53] To verify the performance of nPCU NPs against hypoxia and ensure the treatment is synergistic, the phototherapeutic efficiency of nPCU NPs and PpIX under both normoxic and hypoxic conditions was investigated for comparison. The cell hypoxia was induced by adding cobalt dichloride in accordance with the reported protocol.[54] After exposure to 50 mW/cm^2 635-nm laser for 3 min, the therapeutic efficiencies of PpIX and nPCU under hypoxic ("H") and normoxic ("N") conditions were evaluated by MTT assay (**Fig. 5d**). Notably, the hypoxic cells treated with 12.5 μg/mL nPCU NPs remain distinctive therapeutic efficacy with a lethality of 71%, although their nomorxic group shows higher cell lethality around 90%. From the comparison, it is apparent that cell hypoxia could almost inhibit the phototoxicity of PpIX at various concentrations. The inhibition of cancer phototherapy was also observed in the cells treated by nPCU NPs with 18 wt% of PpIX (**Fig. S5**), because their dominant PDT effect was likewise suppressed by tumor hypoxia. Additionally, 2',7'-dichlorofluorescein diacetate (DCFH-DA) as a fluorescent probe was used to evaluate the production of intracellular ROS with existence of laser irradiation. As shown in **Fig. 5e**, PpIX and nPCU show green fluorescence, indicating they could generate singlet oxygen to sensitize DCFH-DA in normoxic cells. Whereas, the hypoxia groups of PpIX and nPCU do not display any green fluorescence, demonstrating that successful construction of hypoxic condition can prohibit their production of ROS under irradiation. Therefore, nPCU NPs can provide efficient combinational PDT/PTT against tumor hypoxia.

Conclusions

In conclusion, we have designed and developed a post-synthetic modification method to construct PpIX-conjugated NMOFs without invasive impact on their crystalline structure. Through systematic investigations, we found that the conjugation of PpIX within MOF structure can induce a π-stacking effect, which partly inhibits its singlet oxygen generation and enables photo-thermal conversion. By varying PpIX content, the photoactive properties of nPCU NPs can be tunable to control PDT and PTT efficiencies in combinational phototherapeutic effect triggered by single laser irradiation. The proof-of-concept experiment on DOX delivery further demonstrates that nPCU NPs potentiate serving as a drug delivery system to meet multiple and specialized request of cancer treatment. Moreover, in vitro phototherapy of nPCU NPs provided prominent and synergistic phototherapeutic intervention under both normoxic and hypoxic conditions. Our work presents a reliable and facile strategy to fabricate photoactive NMOFs with tunable PDT and PTT effect, which have great potential to boost phototherapeutic efficacy and

overcome tumor heterogeneity for clinical development of cancer phototherapy.

Conflicts of interest

There are no conflicts to declare.

Acknowledgements

The authors are grateful for the support from General Research Fund of Hong Kong (GRF CityU 11306717).

Notes and references

1 P. Rai, S. Mallidi, X. Zheng, R. Rahmanzadeh, Y. Mir, S. Elrington, A. Khurshid and T. Hasan, *Advanced Drug Delivery Reviews*, 2010, **62**, 1094–1124.
2 M. Abbas, Q. Zou, S. Li and X. Yan, *Advanced Materials*, 2017, **29**, 1605021.
3 R. Bonnett, *Chem. Soc. Rev.*, 1995, **24**, 19–33.
4 S. S. Lucky, K. C. Soo and Y. Zhang, *Chem. Rev.*, 2015, **115**, 1990–2042.
5 X. Song, Q. Chen and Z. Liu, *Nano Res.*, 2015, **8**, 340–354.
6 L. Zou, H. Wang, B. He, L. Zeng, T. Tan, H. Cao, X. He, Z. Zhang, S. Guo and Y. Li, *Theranostics*, 2016, **6**, 762–772.
7 M. Ferrari, *Nat Rev Cancer*, 2005, **5**, 161–171.
8 M. E. Davis, Z. (Georgia) Chen and D. M. Shin, *Nat Rev Drug Discov*, 2008, **7**, 771–782.
9 K. Yang, H. Xu, L. Cheng, C. Sun, J. Wang and Z. Liu, *Adv. Mater.*, 2012, **24**, 5586–5592.
10 J. Tu, T. Wang, W. Shi, G. Wu, X. Tian, Y. Wang, D. Ge and L. Ren, *Biomaterials*, 2012, **33**, 7903–7914.
11 L. Wang, Q. Sun, X. Wang, T. Wen, J.-J. Yin, P. Wang, R. Bai, X.-Q. Zhang, L.-H. Zhang, A.-H. Lu and C. Chen, *J. Am. Chem. Soc.*, 2015, **137**, 1947–1955.
12 Q. Zou, M. Abbas, L. Zhao, S. Li, G. Shen and X. Yan, *J. Am. Chem. Soc.*, 2017, **139**, 1921–1927.
13 M. Höckel and P. Vaupel, *J Natl Cancer Inst*, 2001, **93**, 266–276.
14 M. R. Junttila and F. J. de Sauvage, *Nature*, 2013, **501**, 346–354.
15 K. J. Son, H.-J. Yoon, J.-H. Kim, W.-D. Jang, Y. Lee and W.-G. Koh, *Angew. Chem. Int. Ed.*, 2011, **50**, 11968–11971.
16 A. Zhu, K. Miao, Y. Deng, H. Ke, H. He, T. Yang, M. Guo, Y. Li, Z. Guo, Y. Wang, X. Yang, Y. Zhao and H. Chen, *ACS Nano*, 2015, **9**, 7874–7885.
17 Y. Wang, Y. Xie, J. Li, Z.-H. Peng, Y. Sheinin, J. Zhou and D. Oupický, *ACS Nano*, 2017, **11**, 2227–2238.
18 Q. Pei, X. Hu, X. Zheng, S. Liu, Y. Li, X. Jing and Z. Xie, *ACS Nano*, 2018, **12**, 1630–1641.
19 M. Macháček, K. A. Carter, F. Kostelanský, D. Miranda, A. Seffouh, J. Ortega, T. Šimůnek, P. Zimčík and J. F. Lovell, *J. Mater. Chem. B*, 2018, **6**, 7298–7305.
20 G. Pasparakis, T. Manouras, M. Vamvakaki and P. Argitis, *Nature Communications*, 2014, **5**, 3623.
21 W.-H. Chen, G.-F. Luo, Q. Lei, S. Hong, W.-X. Qiu, L.-H. Liu, S.-X. Cheng and X.-Z. Zhang, *ACS Nano*, 2017, **11**, 1419–1431.
22 J. Liu, Q. Chen, L. Feng and Z. Liu, *Nano Today*, 2018, **21**, 55–73.
23 Z. Sheng, D. Hu, M. Zheng, P. Zhao, H. Liu, D. Gao, P. Gong, G. Gao, P. Zhang, Y. Ma and L. Cai, *ACS Nano*, 2014, **8**, 12310–12322.
24 G. Feng, Y. Fang, J. Liu, J. Geng, D. Ding and B. Liu, *Small*, 2017, **13**, 1602807.
25 C. Yang, Y. Chen, W. Guo, Y. Gao, C. Song, Q. Zhang, N. Zheng, X. Han and C. Guo, *Advanced Functional Materials*, 2018, **28**, 1706827.
26 J. Li, C. Xie, J. Huang, Y. Jiang, Q. Miao and K. Pu, *Angewandte Chemie International Edition*, 2018, **57**, 3995–3998.
27 H. Zhu, J. Li, X. Qi, P. Chen and K. Pu, *Nano Letters*, 2018, **18**, 586–594.
28 X. Zhen, C. Xie and K. Pu, *Angewandte Chemie International Edition*, 2018, **57**, 3938–3942.
29 P. Horcajada, T. Chalati, C. Serre, B. Gillet, C. Sebrie, T. Baati, J. F. Eubank, D. Heurtaux, P. Clayette, C. Kreuz, J.-S. Chang, Y. K. Hwang, V. Marsaud, P.-N. Bories, L. Cynober, S. Gil, G. Férey, P. Couvreur and R. Gref, *Nat Mater*, 2010, **9**, 172–178.
30 P. Horcajada, R. Gref, T. Baati, P. K. Allan, G. Maurin, P. Couvreur, G. Férey, R. E. Morris and C. Serre, *Chem. Rev.*, 2012, **112**, 1232–1268.
31 M.-X. Wu and Y.-W. Yang, *Advanced Materials*, 2017, **29**, 1606134.
32 K. Lu, C. He and W. Lin, *J. Am. Chem. Soc.*, 2014, **136**, 16712–16715.
33 S.-Y. Li, H. Cheng, B.-R. Xie, W.-X. Qiu, J.-Y. Zeng, C.-X. Li, S.-S. Wan, L. Zhang, W.-L. Liu and X.-Z. Zhang, *ACS Nano*, 2017, **11**, 7006–7018.
34 J. Park, Q. Jiang, D. Feng, L. Mao and H.-C. Zhou, *J. Am. Chem. Soc.*, 2016, **138**, 3518–3525.
35 M. Lismont, L. Dreesen and S. Wuttke, *Advanced Functional Materials*, 2017, **27**, 1606314.
36 Y. Zhang, F. Wang, C. Liu, Z. Wang, L. Kang, Y. Huang, K. Dong, J. Ren and X. Qu, *ACS Nano*, 2018, **12**, 651–661.
37 W. Zhang, J. Lu, X. Gao, P. Li, W. Zhang, Y. Ma, H. Wang and B. Tang, *Angewandte Chemie*, 2018, **130**, 4985–4990.
38 J.-Y. Zeng, M.-K. Zhang, M.-Y. Peng, D. Gong and X.-Z. Zhang, *Advanced Functional Materials*, 2018, **28**, 1705451.
39 W. Wang, L. Wang, Y. Li, S. Liu, Z. Xie and X. Jing, *Advanced Materials*, 2016, **28**, 9320–9325.
40 X. Zheng, L. Wang, Q. Pei, S. He, S. Liu and Z. Xie, *Chem. Mater.*, 2017, **29**, 2374–2381.
41 A. Schaate, P. Roy, A. Godt, J. Lippke, F. Waltz, M. Wiebcke and P. Behrens, *Chem. Eur. J.*, 2011, **17**, 6643–6651.
42 I. Hamachi, Y. Tajiri, T. Nagase and S. Shinkai, *Chemistry – A European Journal*, 1997, **3**, 1025–1031.
43 Q. Tian, F. Jiang, R. Zou, Q. Liu, Z. Chen, M. Zhu, S. Yang, J. Wang, J. Wang and J. Hu, *ACS Nano*, 2011, **5**, 9761–9771.
44 C. He, K. Lu, D. Liu and W. Lin, *J. Am. Chem. Soc.*, 2014, **136**, 5181–5184.
45 X. Gong, T. Milic, C. Xu, J. D. Batteas and C. M. Drain, *J. Am. Chem. Soc.*, 2002, **124**, 14290–14291.
46 K. A. Carter, S. Shao, M. I. Hoopes, D. Luo, B. Ahsan, V. M. Grigoryants, W. Song, H. Huang, G. Zhang, R. K. Pandey, J. Geng, B. A. Pfeifer, C. P. Scholes, J. Ortega, M. Karttunen and J. F. Lovell, *Nature Communications*, 2014, **5**, ncomms4546.
47 K. Lu, C. He and W. Lin, *J. Am. Chem. Soc.*, 2015, **137**, 7600–7603.
48 Y. Jiang, J. Li, X. Zhen, C. Xie and K. Pu, *Advanced Materials*, 2018, **30**, 1705980.
49 C. M. Hessel, V. P. Pattani, M. Rasch, M. G. Panthani, B. Koo, J. W. Tunnell and B. A. Korgel, *Nano Lett.*, 2011, **11**, 2560–2566.
50 M. Dominska and D. M. Dykxhoorn, *J Cell Sci*, 2010, **123**, 1183–1189.

View Article Online
DOI: 10.1039/C9TB01154D

51 L. M. P. Vermeulen, S. C. De Smedt, K. Remaut and K. Braeckmans, *European Journal of Pharmaceutics and Biopharmaceutics*, 2018, **129**, 184–190.
52 W. R. Wilson and M. P. Hay, *Nature Reviews Cancer*, 2011, **11**, 393.
53 B. W. Henderson and V. H. Fingar, *Cancer Res*, 1987, **47**, 3110–3114.
54 T. Uchida, F. Rossignol, M. A. Matthay, R. Mounier, S. Couette, E. Clottes and C. Clerici, *J. Biol. Chem.*, 2004, **279**, 14871–14878.

View Article Online
DOI: 10.1039/C9TB01154D

Novel photoactive metal-organic framework nanoparticles were developed via facile post-synthetic conjugation method to achieve tunable combinational PDT and PTT.